Nuclear Instruments and Methods in Physics Research A 806 (2016) 146–153

Contents lists available at ScienceDirect

Nuclear Instruments and Methods in Physics Research A

journal homepage: www.elsevier.com/locate/nima

Source of slow polarized positrons using the brilliant gamma beam at ELI-NP. Converter design and simulations

Nikolay Djourelov *, Andreea Oprisa, Victor Leca

Extreme Light Infrastructure-Nuclear Physics, Horia Hulubei National Institute for Physics and Nuclear Engineering, 30 Reactorului Street, P.O. Box MG-6, Magurele, 077125 Ilfov County, Romania

ARTICLE INFO

Article history:
Received 15 July 2015
Received in revised form
11 September 2015
Accepted 3 October 2015
Available online 22 October 2015

Keywords:
Gamma beam
Slow positron beam
Polarized positrons
Simulation

ABSTRACT

Simulations of slow positron (e_s^+) source based on interaction of a circularly polarized gamma beam with a W converter were performed. The aim of the study was to propose a converter geometry and to determine the expected slow positron beam intensity and its spot size, and the degree of positron spin polarization, as well. The Monte Carlo simulations by means of GEANT4 were used to estimate the fast positron production and the moderation efficiency of the converter working as a self-moderator, as well. Finite element analysis by means of COMSOL Multiphysics was applied to calculate the fraction of extracted moderated positrons from the converter cells and the quality of the beam formation by focusing. Using the low energy (<3.5 MeV) gamma beam at ELI-NP with intensity of $2.4\times10^{10}\gamma$/s the production of a slow positron beam with intensity of $1–2\times10^{6}e_s^+$/s is predicted. For the optimized converter geometry and in case of 100% circular polarization of the gammas the degree of spin polarization of the slow positron beam is expected to be 33%.

1. Introduction

High intensity slow positron beams find wide application in solid state and surface physics, and in material science. An intense beam is desirable in order to reduce spectrum acquisition time or to improve statistics, and also for brightness enhancement. Therefore, great efforts have been made to generate positrons by the (γ, e^+e^-) reaction using bright γ-sources. Such sources are based on bremsstrahlung in a target at electron linear accelerators [1–4], while at nuclear reactors are based on either γ-radiation from nuclear fission [5] or on high-energy prompt γ-rays after thermal neutron capture [6,7]. Another approach is to utilize a γ-beam. Estimates of the intensity and the brightness of such positron sources at different converter geometries are published in [8]. At Extreme Light Infrastructure-Nuclear Physics (ELI-NP) facility in Magurele, near Bucharest, Romania, low (<3.5 MeV) and high (<20 MeV) energy γ-beams with low emittance are planned to be created by inverse Compton scattering of photons, provided by a high-power laser, with an electron beam, provided by a Linac. While both γ-beams will be used mainly for nuclear physics studies, only the low energy γ-beam will be used for slow or moderated positron (e_s^+) production [9].

Polarization of e_s^+ was discovered by Zitzewitz et al. in 1979 [10]. Spin-polarized e_s^+ provide a new, atomic scale view on the magnetism and on the electronic structure of magnetic materials. Van House et al. [11] have studied e^+ moderation process with e_s^+ beam based on ^{22}Na source, with electrostatic guidance and a degree of polarization $P=(48\pm2)$%. Maekawa et al. build a similar e_s^+ beam using a ^{68}Ge–^{68}Ga e^+ source produced from the ^{69}Ga (p,2 n)^{68}Ge nuclear reaction by irradiating a GaN substrate with 20 MeV protons for 400 h in 20 cyclotron sessions [12]. The achieved beam intensity was $5\times10^{3}e_s^+$/s. The degree of spin polarization of the e_s^+ beam was determined to be (47 ± 8)% from the magnetic field dependence of the *para*-Positronium intensity in fused silica.

A few other methods to produce polarized e^+ are being considered by the linear collider community. The concept is to use e^+e^- pairs created by converting circularly polarized γ-rays. The circularly polarized γ-rays may come from one of these processes: helical undulator radiation by unpolarized electron beams [13], Compton scattering of circularly polarized laser-light off a high-energy electron beam [14,15] (a process that will be used also within the ELI-NP project), and Bremsstrahlung of longitudinally polarized electrons in high-Z amorphous targets [16].

The purpose of the present paper is to report on the optimization of the converter geometry for high intensity slow positron beam. We report results of Monte Carlo simulations of the fast positron production and their moderation in a converter using the GEANT4.10.01.p01 code [17]. The polarization transfer from

* Corresponding author.
E-mail address: nikolay.djourelov@eli-np.ro (N. Djourelov).

http://dx.doi.org/10.1016/j.nima.2015.10.009
0168-9002/

circularly polarized gammas to the spin of moderated positrons was tracked also by GEANT4. In addition finite element analysis by COMSOL Multiphysics [18] was used to calculate the fraction of moderated positrons which can be extracted from the converter cells.

2. Low energy γ-beam characteristics at ELI-NP

The possibility for a positron source based on γ-beam at ELI-NP was mentioned for the first time in the ELI-NP project White book [9]. Hugenschmidt et al. also described the features of positron sources based on γ-beams [8]. In the last publication, the parameters, γ-rays of energy 2.5(5) MeV with beam diameter of few hundreds of μm and intensity of $10^{15}\gamma$/s, were taken from the ELI-NP White book and used for estimations. Based on these values, they concluded that the positron source at ELI-NP could be designed in high intensity or high brightness modes and it would be superior over the existing or planned slow positron sources worldwide.

With the development of the project, new and detailed information becomes available about the parameters of the Gamma Beam System (GBS) at ELI-NP published by the designer of the machine, the EuroGammaS association [19]. The macro bunches will be provided with a repetition rate of 100 Hz, and each macro bunch will consists of 32 micro bunches of ~1 ps, separated by 16 ns gaps. The number of γ-rays in a bunch will be 7.45×10^6 which results in time averaged intensity of $I_\gamma = 2.38\times10^{10}\gamma$/s. The data concerning the γ-beam energy and divergence characteristics at the low energy interaction point (IP) are provided by simulations of collision at the IP of an intense high power laser beam and a high brightness electron beam. At the IP the γ-beam spot has a rms radius of 25 μm. Very important is the correlation between the γ-ray energy and their momentum direction. The polar angle with the beam axis is plotted in Fig. 1. The correlation indicates that a collimator with aperture equivalent to polar angle cut of ~2.7 mrad can successfully filter the unwanted γ-rays with energy bellow 1.022 MeV, which may contribute to converter temperature increase but not to pair production. The GBS design determines that the distance between the low energy IP and a target to act as γ-to-e^+ converter is of the order of 4 m. Thus, a collimator can be placed at a distance, for example, of 3.5 m from the IP and has to be with an aperture of 19 mm. GEANT4 simulation of such geometry showed that the FWHM of the γ-beam intensity profile at 4 m from the IP is D_γ= 6.1 mm, that 33.5% of the γ-rays are stopped by the collimator and the rest interacted with a solid tungsten target 12-cm-thick along the beam propagation direction. The polar angle distribution of the momentum direction of the created fast e^+ in the target is plotted in Fig. 2. The mean value of the fast e^+ energy distribution shown in Fig. 3 is E_+^{mean} = 0.859 MeV.

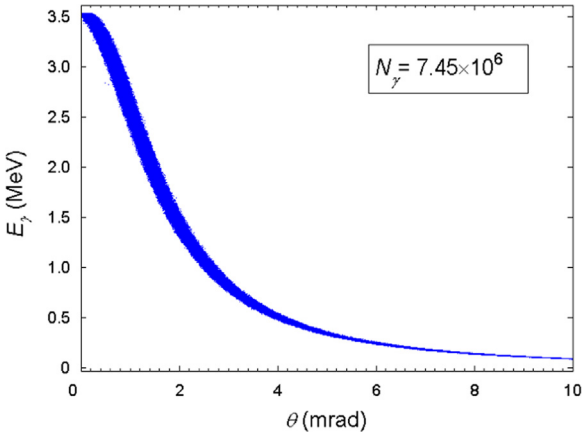

Fig. 1. Energy versus scattered angle, θ, of the γ-rays at the interaction point.

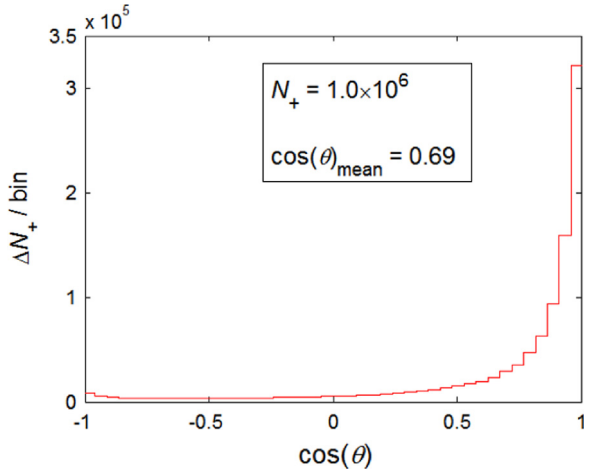

Fig. 2. The polar angle distribution of the momentum direction of the created fast e^+ in a solid W target 12-cm-thick along the γ-beam propagation direction.

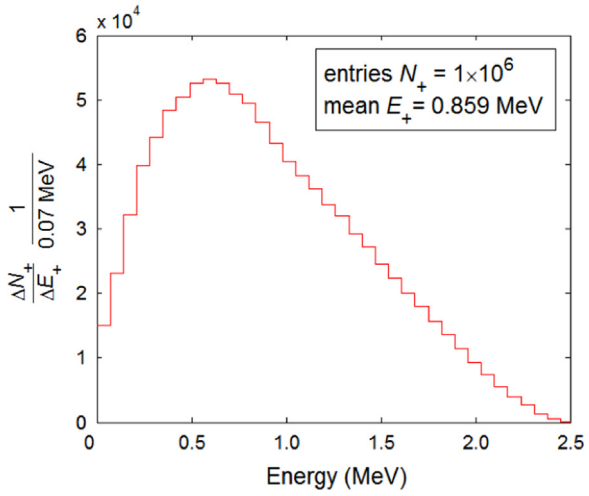

Fig. 3. Energy spectrum of the created fast e^+ in a solid W target 12-cm-thick along the γ-beam propagation direction.

3. Converter geometry

Various geometry designs and options for the converter and moderator materials are reviewed in [20]. Two of these designs (Venetian blinds and a single foil) were discussed by Hugenschmidt et al. as candidates to achieve high brightness and high intensity positron source for ELI-NP [8]. However, the high brightness design is not reasonable to be implemented due to the fact that the γ-beam will have an intensity 4 orders of magnitude lower than initially estimated in the White Book, with the beam spot 2 orders of magnitude larger at the converter as compared to what was considered initially. Due to the high γ-radiation environment around the converter we have chosen for the high intensity design to use a tungsten converter which will work in self-moderation mode. A design of such converter/moderator is a complex process of geometry parameters optimization. A converter with high mass is desirable for high production of fast positrons while high surface-to-volume ratio would lead to efficient moderation of the fast e^+. Another important issue to be considered is the extraction of the e_s^+.

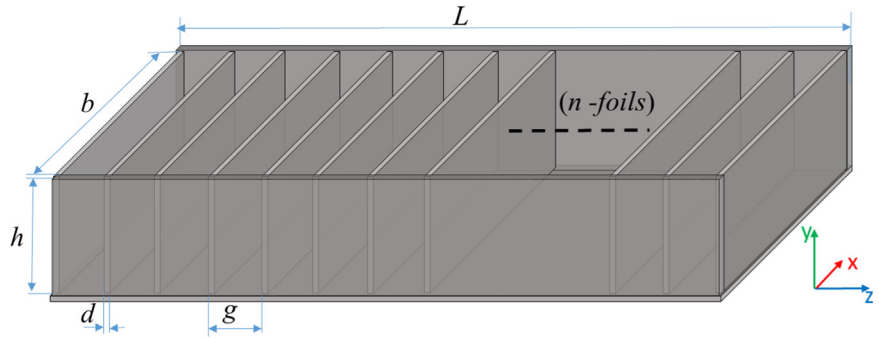

Fig. 4. One-side-open Venetian blind geometry of the proposed CMA (converter/moderator assembly). The γ-beam propagates along z-axis.

Venetian blind or its modifications, such as honey comb, are well-known as efficient moderator geometries [20–22] and used as converter/moderator as well [7,23]. Due to the small divergence of the γ-beam and almost forward momentum direction of the fast e^+ (Fig. 2) one-direction-elongated shape of the converter/moderator assembly (CMA) has to be considered. Such CMA will consists of n number of W foils of thickness d with a spacing g between the adjacent foils (see Fig. 4). Due to the fact that moderation can be more efficient in reflection mode [24], two side and a bottom walls are added. The width b and height h of the W foils is natural to be of the order of the γ-beam spot diameter and at the same time the ratio $\xi = \frac{h}{g}$ has to be kept low for successful extraction of the slow positrons, which will be discussed in Section 4.3. The diameter of the γ-to-e^+ converters of the positron sources based on nuclear reactors is 10–25 cm, as limited by the diameters of the channels leading to the reactor core, resulting in FWHM of the diameter of the primary e_s^+ beam of 10–25 mm [6,7,23,25]. For ELI-NP case there is no such technical restriction on L. The cumulative thickness $\delta = nd$ of the CMA determines the γ-beam absorption. However, the CMA length $L = n(g+d)$ has to be restricted to a reasonable value due to focusing reasoning. The length of the CMA together with momentum and angular divergence of the extracted e_s^+ are the main factors which determine the diameter of the formed primary e_s^+ beam. Our choice is to fix $L = 300$ mm with a goal to have a primary e_s^+ beam with FWHM in diameter of 25 mm. For a fixed L, from the requirement of low ξ follows that b cannot be very small and hence the number of foils n will have an upper limit which may lead to incomplete γ-beam absorption. Therefore, the CMA sizes need optimization.

4. Results and discussion

4.1. Simulation of e^+ moderation

Energetic e^+, after implanted in matter, slow down to the thermal energy of about 25 meV due to elastic and inelastic scattering. Thermalized e^+ start to diffuse and eventually annihilate with an electron. However, a small fraction of them can reach the surface of the material and in case the material has a negative positron work function (e.q., $\Phi^+ = -3.0$ eV, for (110) tungsten) they emerge from the surface with an energy $\mathcal{E}_+ = |\Phi^+|$.

One practical way to estimate the moderation efficiency of a moderator is to calculate the fraction of e^+ which are implanted into a thin subsurface layer with thickness of the order of the e^+ effective diffusion length, L_+, and to consider that the e^+ which do not form Positronium will be emitted as moderated [8,21]. It is easily applicable in case of monoenergetic fast e^+ and simple moderator geometry. However, simulation is necessary for complex e^+ energy spectrum and moderator geometry. Such approach was used and implemented in the EGS4 code, where the authors simulate both implantation and diffusion processes [26].

Although GEANT4 does not cover the physics for particle energies < 50 eV, the e^+ implantation profile can be simulated with acceptable precision [27]. As a matter of fact an uncertainty of 50 eV for e^+ with energies of few hundred keV leads to uncertainty of few nm in the average implantation depth (in W) which is two orders of magnitude shorter than $L_+ = 135$ nm in W [28]. In our GEANT4 simulation the fast e^+ are tracked until they reach energy < 25 meV in a target. Then we mimic the final step in the process of e^+ moderation. It consists of the following. The distance to the nearest target surface, z, is found and with a probability of $P = B\exp(-z/L_+)$ this positron is forced to move (by killing the track of the tracked positron and creating a new one) on the surface out of the target with momentum normal to the surface and energy of $\mathcal{E}_+$. The fate of a thermalized e^+ on a surface is reemission into vacuum, Positronium formation or annihilation. In the P formula, the surface branching ratio of e^+ reemission for W is $B \approx 0.4$ [29], while the exponential factor describes the probability the e^+ to travel the distance z due to diffusion.

For validation reasons, the geometries for the W-foil moderators and the e^+ sources described in [28], in transmission, and in [24], in reflection mode, were reproduced. In the simulations the corresponding e^+ energy spectra of ^{22}Na and ^{58}Co were used. The moderation efficiencies of 6.1×10^{-4} (transmission mode) and 2.8×10^{-3} (reflection mode) obtained by our GEANT4 simulations agree satisfactorily with the experimental ones of 4×10^{-4} and 3.8×10^{-3}, respectively.

4.2. Optimization of the CMA parameters

In general, the optimization of the CMA parameters against the best γ-to-e_s^+ conversion efficiency can be done directly with GEANT4 simulation developed by us. However, due to the long GEANT4 computing time a preliminary estimation of some of the initial parameters was necessary. For few-MeV-gammas the optimum thickness of a single converter W foil with highest amount of emitted e^+ is ~ 0.2 mm [30] and it can be considered as the upper limit for single foil thickness for CMA. The fraction of γ-rays which interact with the CMA can be expressed by the product $\Gamma_{int}(h,b,D_\gamma,\delta) = \Gamma_{cs}(h,b,D_\gamma)\Gamma_{abso}(\delta)$, where represents the fraction of γ-rays which hit the front side of the CMA, the intensity profile of the γ-beam is represented for simplicity with a Gaussian having FWHM equal to D_γ, and $\Gamma_{abso}(n,d) = 1 - exp(-\mu\delta)$ is the γ-rays absorption probability with linear attenuation coefficient $\mu = 0.043$ mm^{-1} for $E_\gamma = 2.5$ MeV [31]. The cumulative thickness can be expressed as $\delta = \frac{Ld}{\left(\frac{h}{\xi}+d\right)}$ and for fixed L and ξ is a function of h and d.

The fraction of absorbed γ-rays, $\Gamma_{int}(h,b,D_\gamma,\delta)$, as a function of CMA height, h, at few values of foil thickness, d, and CMA width, b,

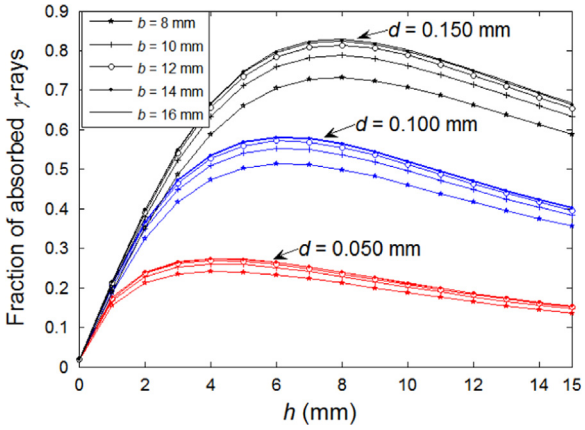

Fig. 5. The fraction of absorbed γ-rays, $\Gamma_{int}(h,b,D_\gamma,\delta)$, as a function of CMA height, h, for different values of foil thickness, d, and different CMA width, b. The CMA length is fixed $L=300$ mm, while the CMA cell aspect ratio is $\xi=3$.

Table 1
The absolute γ-to-e_s^+ conversion efficiency, Γ, at selected values for the CMA height, h, and foil thickness, d, for CMA with width $b=16$ mm and length $L=300$ mm, and γ-beam intensity profile with $D_\gamma=6.1$ mm as obtained by GEANT4 simulation. The statistical error in determination of Γ was 0.3×10^{-5}.

h (mm) d (mm)	5	6	7	8
0.06	7.4×10^{-5}	7.6×10^{-5}	7.5×10^{-5}	7.3×10^{-5}
0.07	7.5×10^{-5}	7.7×10^{-5}	7.6×10^{-5}	7.5×10^{-5}
0.08	7.8×10^{-5}	8.2×10^{-5}	8.1×10^{-5}	7.6×10^{-5}
0.09	7.4×10^{-5}	7.4×10^{-5}	7.2×10^{-5}	7.0×10^{-5}

fixed CMA length $L=300$ mm, and CMA cell aspect ratio $\xi=3$ (the choice of this value is discussed in Section 4.3) is plotted in Fig. 5. The results show that for best γ-rays absorption $b\geq12$ mm and $h\approx4-8$ mm. Also, the decrease of the foil thickness leads to decrease of the amount of the absorbed γ-rays or less fast e^+, however, for best γ-to-e_s^+ conversion such decrease may be compensated by better moderation.

The final optimization step against the best γ-to-e_s^+ conversion efficiency was done by GEANT4 simulation for γ-beam with characteristics described in Section 2, directly irradiating the CMA at 4 m, with CMA design as shown in Fig. 4 for different values of h and d, as presented in Table 1. Only those e_s^+ which emerge from the internal walls of the CMA were counted. Consequently, the intensity of e_s^+ that can be obtained by the proposed CMA design is $I_{e_s^+}=\Gamma_{best}I_\gamma=1.95\times10^6 e_s^+/\mathrm{s}$, where $\Gamma_{best}=8.2\times10^{-5}$ is the best efficiency value as determined from the data given in Table 1.

4.3. Extraction of moderated positrons

One of the critical points in the converter design is the extraction of e_s^+. Problems appear due to the short distances between the foils and, consequently, of screening of the electric field applied for extraction of the e_s^+. Simulations with COMSOL [18] were performed for one representative cell of the converter and an extraction mesh placed at 3 mm from the converter as shown in Fig. 6a. The e_s^+ are emitted with an initial energy of $\mathcal{E}_+$ normally and uniformly from the internal surface of the cell. For more realistic simulation we have specified that the surface can reflect low energy e^+ with a probability of 0.6, otherwise they annihilate [32]. The potential difference between the CMA and the extraction mesh is set to $U=60$ V. The simulation results showed that about 40% of the e_s^+ are extracted. Due to lack of electric field gradient the e_s^+ emitted from the lower part of the transversal walls do not have chance to be extracted.

The three basic ways to achieve better electric field gradient to extract e_s^+ are to decrease the aspect ratio, to make segmentation of the transversal foils [33], and/or to increase the potential difference U. In Fig. 7 the fraction of extracted e_s^+ together with the FWHM of their energy spread (in this case is roughly approximated by a Gaussian) as a function of the applied potential difference between the extraction mesh and the CMA for non-segmented converter with $h=6$ mm, $b=16$ mm and $\xi=3$ as obtained by COMSOL simulation is plotted. It can be seen that high potential is needed for successful extraction. However, it comes with significant increase of the energy spread which has to be taken into account together with the divergence for the subsequent beam formation by focusing. In order to have consistency with the focusing system (see Section 4.4) we consider a CMA design (segmented or none) as good when the energy spread of the extracted e_s^+ does not exceed 60 eV.

It has to be mentioned that the temperature change of the CMA due to the interaction with γ-rays was also studied. The power of the energy deposited in CMA obtained by GEANT4 was 1.5 mJ/s, which resulted (as done by COMSOL simulations not included in the text) that the maximum CMA temperature will exceed the ambient temperature by less than 2 °C.

The electric field equipotential lines and the e_s^+ trajectories for a segmented into 6 CMA are plotted in Fig. 6b. The segmentation effect on the creation of electric field gradient to extract e_s^+ towards the extraction mesh is clearly seen. The effect of the number of segments on the extraction efficiency is shown in Fig. 8. The method of segmentation is very effective achieving more than twice (81%, for 6 segments, and $U=60$ V) extraction efficiency as compared to the non-segmented converter. At the same time, the width of the energy spread is ~40 V and it corresponds approximately to $U=600$ V in the case of non-segmented CMA, for which ~62% of the e_s^+ can be extracted (see Fig. 7). It is worth noting that a segmented converter could be easily forced to act as non-segmented by making electrical contact between the segments.

The fraction of extracted e_s^+ can be improved by decreasing the gap aspect ratio ξ, which is demonstrated in Fig. 9. However, for a CMA with fixed length and height a lower ξ leads to less number of the transversal foils and for a fixed foil thickness it results to less number of produced e_s^+ on the CMA surface. The combined production and extraction efficiency of e_s^+ as a function of ξ (see Fig. 9) shows rather wide maxima. A decrease in the combined efficiency occurs from $\xi\cong3$.

4.4. Beam formation by focusing

The e_s^+ extracted from the CMA will be focused by a system of electrostatic lenses. The beam formation focusing system is copied from the PULSTAR slow positron source [7]. The original lenses have been designed for focusing of e_s^+ which exit the extraction mesh with longitudinal energy of up to 60 eV. The system has been tested with electron guns out of reactor core [34] and also in operational conditions [7]. The authors succeeded to focus the e_s^+ emitted from a converter with diameter of 24 cm into a beam with diameter with FWHM=2 cm and demonstrated excellent agreement between simulation and experimental results on focusing. For our system we just scaled the original radii by a factor of 1.25. Thus the internal diameters of the lenses are 30.5, 25, 19.5, 14, 12.5, and 9.4 cm (see Fig. 10, top). The voltages applied to the lenses are 920, 800, 735, 50, −3100, 640 V. The extraction mesh was kept at 910 V and the solenoid at 0 V. The electromagnetic field (see Fig. 10, bottom) and the e_s^+ trajectories (see their projections on the x–y and y–z planes in Fig. 11 top and bottom, correspondingly)

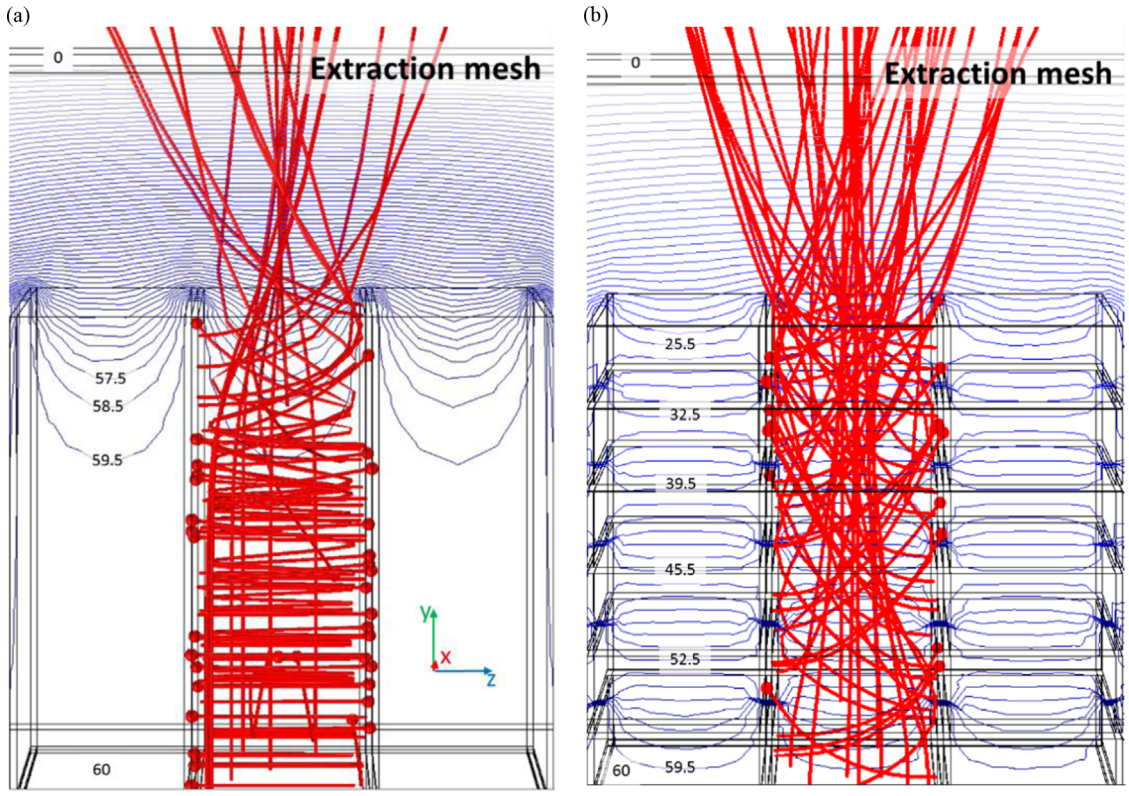

Fig. 6. The electric field and e_s^+ trajectories in a cell of the CMA at $U=60$ V and extraction mesh at ground. The CMA is with the optimized sizes (see Section 4.2). The equipotential lines are drawn at every 1 V on the y–z intersecting the converter in the middle. The points mark annihilation events. The extraction mesh is at distance of 3 mm from the converter. In the case (b) of segmented CMA only the bottom segment is at potential U, while the rest are at floating potential.

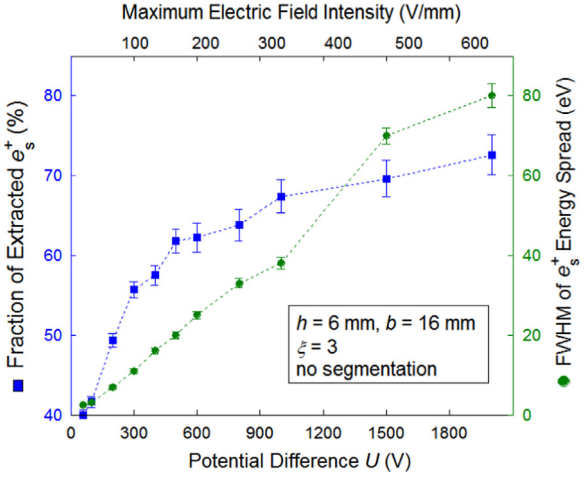

Fig. 7. The fraction of extracted e_s^+ and the FWHM of their energy spread as a function of the applied potential difference between the CMA and the extraction mesh. The CMA is with the optimized sizes (see Section 4.2). The extraction mesh is at a distance of 3 mm from the converter.

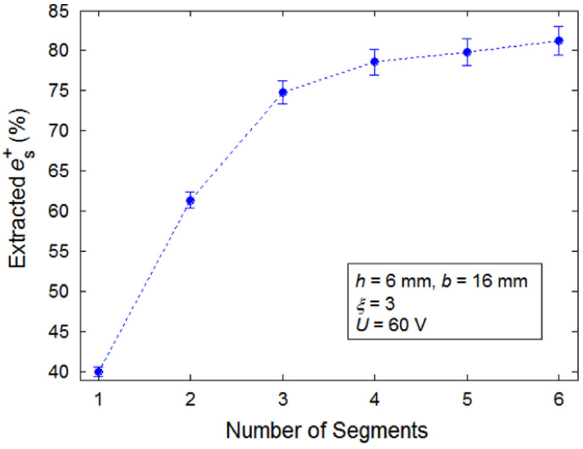

Fig. 8. The fraction of extracted e_s^+ as a function of the number of CMA segments. The CMA is with the optimized sizes (see Section 4.2). The extraction mesh is at distance of 3 mm from the converter.

were simulated by COMSOL. As input values of the e_s^+ energy spread and divergence we used the one obtained as output in the simulation of the e_s^+ extraction from the CMA. The results show that (92 ± 1)% of the extracted e_s^+ will be transmitted to the transport beamline, and the diameter of the e_s^+ beam will have FWHM = 2.5 cm.

4.5. Spin polarized positrons

The production of highly polarized short-pulse positrons has been obtained experimentally for the first time at KEK, Japan [15]. There, Omori et al. have demonstrated that by using a circularly polarized laser beam of 532 nm scattered off a high-quality, 1.28 GeV electron beam, the formed circularly polarized γ-beam leads to creation of polarized e^+ with an intensity of $2\times10^4 e^+$/bunch, and a degree of polarization of 73%, as determined by means of a newly designed positron polarimeter. The authors also reported a very good agreement with the obtained value of 77%, by GEANT4 simulations, for the spin polarization degree.

The influence of slowly varying electric and magnetic fields on polarized e^- beams is explained in [35]. Few cases are described which for non-relativistic beam can be summarized as follows: (a) deflecting low energy e^- by electric field over an angle of $\pi/2$ change the longitudinal polarization to transversal (or the opposite); (b) acceleration electric field (longitudinal) leaves the e^-

polarization unchanged; (c) transverse magnetic field rotates the direction of the beam at the same rate as the e^- spin, so that a magnetic field leaves the state of transverse polarization unchanged; (d) longitudinal magnetic field does not change the direction and magnitude of the momentum but the spin precesses about the propagation axis. The consequences of these cases are that the e_s^+ z-component of the polarization degree, P_z, will be preserved in the extraction electric field (for the e_s^+ which emerge from the transversal foils it will be changed from longitudinal to transversal), then the electrostatic focusing will not change the direction or the degree of the polarization. Further, in the transport lines due to the solenoidal magnetic field the e^+ spins will rotate along the solenoid axis but the degree of the transversal beam polarization will be preserved.

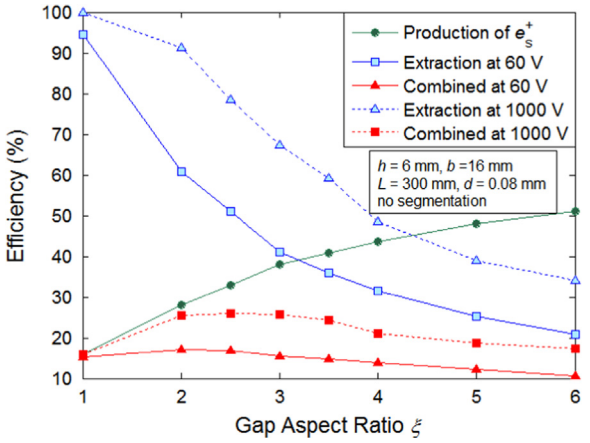

Fig. 9. The e_s^+ production efficiency and the e_s^+ extraction efficiency as a function of the gap aspect ratio ξ for a non-segmented CMA with h=6 mm, b=16 mm, L=300 mm and d=0.08 mm for two potential differences of U=60 V and 1000 V between the CMA and the extraction mesh placed at 3 mm from the CMA. The statistical errors are of the order of twice the marker size.

In order to clarify how the circular polarization of the γ-beam is transferred to e_s^+ spin polarization we performed GEANT4 simulations for the proposed CMA design with sizes optimized for the best moderation efficiency. The COMSOL electric field map for U=60 V was read by GEANT4. The polarization Stock's vectors of the incident γ-rays propagating along the z-axis were set to (0,0,1), i.e. 100% circular polarization. In Fig. 12 the longitudinal polarization, P_z, as a function of the energy of the fast e^+ as created in the bulk of CMA with sizes optimized for best moderation efficiency is presented as a 2D histogram. The degree of the longitudinal polarization is 39% (see, mean P_z in Fig. 12). Also from the plotted results it can be seen that the e^+ with lower energy carry less helicity. Actually, House and Zitzewitz in their study of the moderation process by polarized e^+ came to the same conclusion [11].

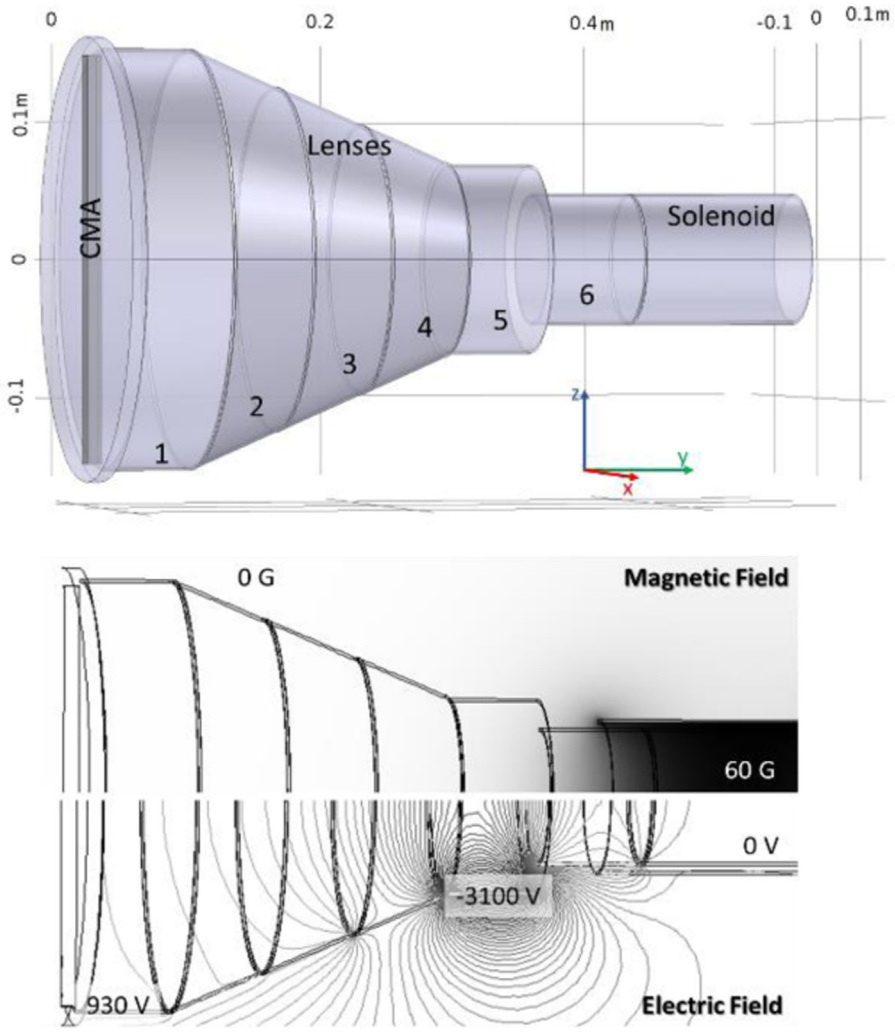

Fig. 10. Geometry and electromagnetic field maps of a system of lenses for beam focusing. Consists of six electrostatic lenses and the beginning of the solenoid for beam transport is also shown.

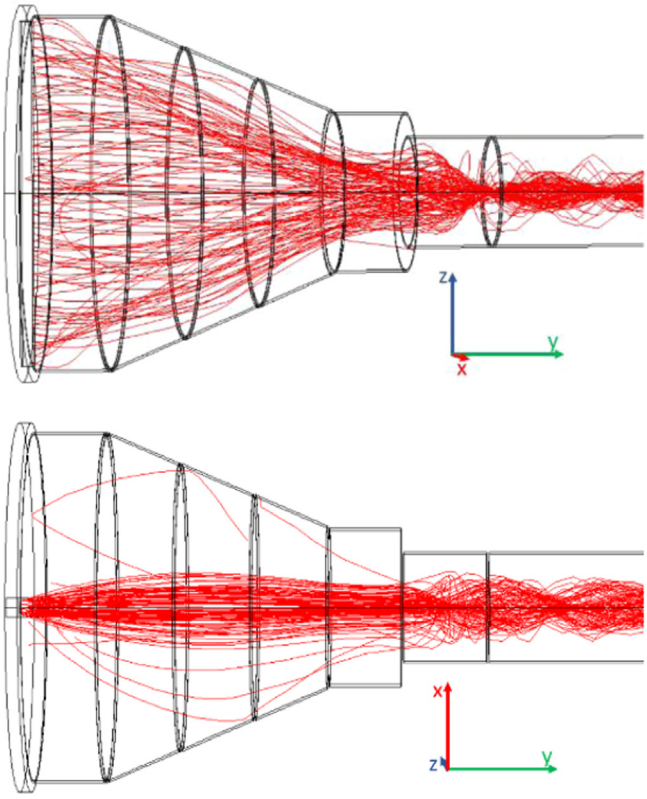

Fig. 11. Trajectories of e_s^+ in the system of lenses with transport solenoid as simulated by COMSOL.

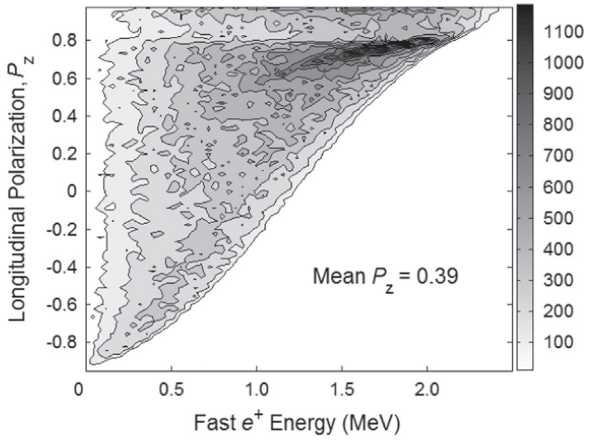

Fig. 12. Longitudinal polarization, P_z, as a function of the energy of the fast e^+ as created in the bulk of CMA with sizes optimized for the best moderation efficiency.

Due to the fact that the low energy e^+ are moderated with higher efficiency compared to the high energy e^+, the obtained degree of polarization of e_s^+ at the moment they emerge from the foil surface was 33%, markedly lower than the one of the fast e^+ as created in the bulk of CMA. Another result which was obtained is that the degree of polarization of e_s^+ was preserved after they pass the extraction mesh.

The effect of the foil thickness, d, on the polarization degree was also studied by simulations. The results of the degree of spin polarization of the e_s^+ which emerge from the foil surface are shown in Fig. 13. The e_s^+ polarization degree slightly increases with increasing d. It is due to the fact that a thicker foil absorbs better the low energy fast e^+, which carry low helicity, and they do not reach the near surface region to emerge as e_s^+. However, this lowers the moderation efficiency, as can be seen in Fig. 13.

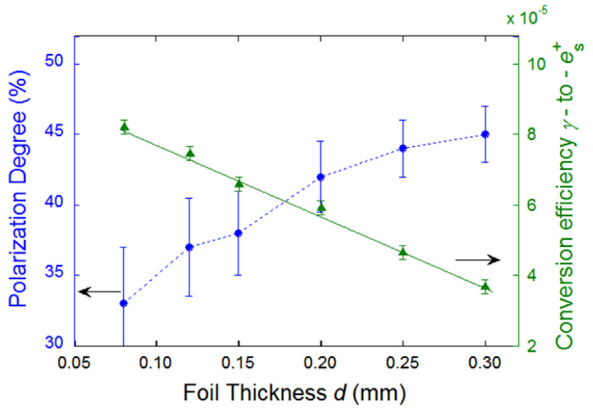

Fig. 13. Degree of polarization of the e_s^+ and CMA conversion efficiency as a function of the foil thickness, d. The all CMA sizes, except for d, are as obtained by the optimization.

5. Conclusions

In this study we have proposed a CMA design for a e_s^+ source to be implemented at ELI-NP. GEANT4 was used to simulate the processes of conversion of the γ-beam into fast e^+. Code to mimic the e^+ diffusion process has been implemented to simulate the final step of e^+ moderation. COMSOL Multiphysics has been applied to study the extraction of e_s^+ from the converter cells and the quality of the beam formation by focusing. The optimization of the CMA sizes against best γ-to-e_s^+ conversion efficiency has been performed. The results show that using the low energy γ-beam at ELI-NP a primary e_s^+ beam with intensity of $1–2\times10^6 e_s^+$/s is achievable. In case that the γ-beam is 100% circularly polarized the degree of spin polarization of the slow positron beam is expected to be 33% for the optimized CMA sizes, and up to 45% for thicker foils.

Acknowledgments

This work is supported by the Project Extreme Light Infrastructure –Nuclear Physics (ELI-NP) –Phase I, a project co-financed by the Romanian Government and the European Union through the European Regional Development Fund, Contract nr. 425/12.12.2012, POS CCE, Axa 2, ID nr. 1334 (ELI-NP) Cod SMIS-CSNR 40741.

References

[1] R.H. Howell, I.J. Rosenberg, M.J. Fluss, Applied Physics A 43 (1987) 247.
[2] T. Hyodo, K. Wada, A. Yagishita, T. Kosuge, Y. Saito, T. Kurihara, T. Kikuchi, A. Shirakawa, T. Sanami, M. Ikeda, S. Ohsawa, K. Kakihara, T. Shidara, Journal of Physics: Conference Series 262 (2011) 012026.
[3] R. Suzuki, T. Ohdaira, T. Mikado, A. Uedono, H. Ohgaki, T. Yamazaki, S. Tanigawa, Materials Science Forum 255–257 (1997) 114.
[4] R. Krause-Rehberg, S. Sachert, G. Brauer, A. Rogov, K. Noack, Applied Surface Science 252 (2006) 3106.
[5] A. van Veen, F. Labohm, H. Schut, J. de Roode, T. Heijenga, P.E. Mijnarends, Applied Surface Science 116 (1997) 39.
[6] C. Hugenschmidt, H. Ceeh, T. Gigl, F. Lippert, C. Piochacz, P. Pikart, M. Reiner, J. Weber, S. Zimnik, Journal of Physics: Conference Series 443 (2013) 012079.
[7] I.H. Ayman, W.G. David, M. Jeremy, G.H. Alfred, M. Saurabh, Journal of Physics: Conference Series 262 (2011) 012024.
[8] C. Hugenschmidt, K. Schreckenbach, D. Habs, P.G. Thirolf, Applied Physics B 106 (2012) 241.
[9] ELI-NP White Book, http://www.eli-np.ro/documents/ELI-NP-WhiteBook.pdf, 2011.
[10] P.W. Zitzewitz, J.C. Van House, A. Rich, D.W. Gidley, Physical Review Letters 43 (1979) 1281.
[11] J. Van House, P.W. Zitzewitz, Physical Review A 29 (1984) 96.

[12] M. Maekawa, Y. Fukaya, A. Yabuuchi, I. Mochizuki, A. Kawasuso, Nuclear Instruments and Methods in Physics Research Section B: Beam Interactions with Materials and Atoms 308 (2013) 9.
[13] V.E. Balakin, A.A. Michailichenko, Preprint INP (1979) 79–85.
[14] A.P. Potylitsin, Nuclear Instruments and Methods in Physics Research Section A: Accelerators, Spectrometers, Detectors and Associated Equipment 398 (1997) 395.
[15] T. Omori, M. Fukuda, T. Hirose, Y. Kurihara, R. Kuroda, M. Nomura, A. Ohashi, T. Okugi, K. Sakaue, T. Saito, J. Urakawa, M. Washio, I. Yamazaki, Physical Review Letters 96 (2006) 114801.
[16] H. Olsen, L.C. Maximon, Physical Review 114 (1959) 887.
[17] GEANT4 -a toolkit for simulation of the passage of particles through matter, version 4.10.01.p01, http://geant4.cern.ch.
[18] COMSOL Multiphysics®, COMSOL 4.3, COMSOL AB, Stockholm, Sweden, 2012.
[19] O.Adriani, S.Albergo, D.Alesini, M.Anania, D.Angal-Kalinin, P.Antici, A.Bacci, R. Bedogni, M.Bellaveglia, C.Biscari, N.Bliss, R.Boni, M.Boscolo, F.Broggi, P.Cardarelli, K.Cassou, M.Castellano, L.Catani, I.Chaikovska, E.Chiadroni, R.Chiche, A. Cianchi, J.Clarke, A.Clozza, M.Coppola, A.Courjaud, C.Curatolo, O.Dadoun, N. Delerue, C.D.Martinis, G.D.Domenico, E.D.Pasquale, G.D.Pirro, A.Drago, F. Druon, K.Dupraz, F.Egal, A.Esposito, F.Falcoz, B.Fell, M.Ferrario, L.Ficcadenti, P. Fichot, A.Gallo, M.Gambaccini, G.Gatti, P.Georges, A.Ghigo, A.Goulden, G.Graziani, D.Guibout, O.Guilbaud, M.Hanna, J.Herbert, T.Hovsepian, E.Iarocci, P. Iorio, S.Jamison, S.Kazamias, F.Labaye, L.Lancia, F.Marcellini, A.Martens, C. Maroli, B.Martlew, M.Marziani, G.Mazzitelli, P.McIntosh, M.Migliorati, A.Mostacci, A.Mueller, V.Nardone, E.Pace, D.T.Palmer, L.Palumbo, A.Pelorosso, F.X. Perin, G.Passaleva, L.Pellegrino, V.Petrillo, M.Pittman, G.Riboulet, R.Ricci, C. Ronsivalle, D.Ros, A.Rossi, L.Serafini, M.Serio, F.Sgamma, R.Smith, S.Smith, V. Soskov, B.Spataro, M.Statera, A.Stecchi, A.Stella, A.Stocchi, S.Tocci, P.Tomassini, S.Tomassini, A.Tricomi, C.Vaccarezza, A.Variola, M.Veltri, S.Vescovi, F.Villa, F. Wang, E.Yildiz, F.Zomer, Technical Design Report EuroGammaS proposal for the ELI-NP Gamma beam System, in: Proceedings of the CORD Conference, 2014.
[20] P.G. Coleman, Positron Beams and their Applications, World Scientific, Singapore, 2000.
[21] V.V. Plokhoi, Y.Z. Kandiev, S.I. Samarin, G.N. Malyshkin, G.V. Baidin, I. A. Litvinenko, V.P. Nikitin, Nuclear Instruments and Methods in Physics Research Section A: Accelerators, Spectrometers, Detectors and Associated Equipment 470 (2001) 44.
[22] B.E. O'Rourke, N. Hayashizaki, A. Kinomura, R. Kuroda, E.J. Minehara, T. Ohdaira, N. Oshima, R. Suzuki, Review of Scientific Instruments 82 (2011) 063302.
[23] A. van Veen, H. Schut, F. Labohm, J. de Roode, Detectors and Associated Equipment 427 (1999) 266.
[24] A. Vehanen, K.G. Lynn, P. Schultz, M. Eldrup, Applied Physics A 32 (1983) 163.
[25] Q. Xu, K. Sato, T. Yoshiie, T. Sano, H. Kawabe, Y. Nagai, K. Nagumo, K. Inoue, T. Toyama, N. Oshima, A. Kinomura, Y. Shirai, Journal of Physics: Conference Series 505 (2014) 012030.
[26] S. Okada, H. Kaneko, Applied Surface Science 85 (1995) 149.
[27] J. Dryzek, P. Horodek, Nuclear Instruments and Methods in Physics Research Section B: Beam Interactions with Materials and Atoms 266 (2008) 4000.
[28] K.G. Lynn, B. Nielsen, J.H. Quateman, Applied Physics Letters 47 (1985) 239.
[29] R. Suzuki, G. Amarendra, T. Ohdaira, T. Mikado, Applied Surface Science 149 (1999) 66.
[30] B. Krusche, K. Schreckenbach, Detectors and Associated Equipment 295 (1990) 155.
[31] J.H. Hubbell, The International Journal of Applied Radiation and Isotopes 33 (1982) 1269.
[32] L.V. Jørgensen, F. Labohm, H. Schut, Av Veen, Journal of Physics: Condensed Matter 10 (1998) 8743.
[33] M. Akihiro, M. Toshinori, Y. Tetsumori, T. Hitoshi, Japanese Journal of Applied Physics 30 (1991) L936.
[34] J.Moxom, A.G.Hathaway, A.I.Hawari, Out of core testing of the North Carolina State University PULSTAR reactor positron beam, in: Proceedings of the IEEE Nuclear Science Symposium Conference Record, NSS'07, 2007, pp. 2343–2348.
[35] H.A. Tolhoek, Reviews of Modern Physics 28 (1956) 277.